Throw Rate Variability on Gravity-Driven Normal Faults; Constraints from the Gudrun Fault, South Viking Graben, Offshore Norway

Christopher A-L. Jackson

Basins Research Group (BRG), Imperial College, Prince Consort Road, LONDON, SW7 2BP, England, UK

email: c.jackson@imperial.ac.uk

ABSTRACT

The growth and throw rate variability on normal faults can reflect fault interaction, plate tectonic forces and, in gravity-driven systems, variations in sediment loading. Because earthquakes may occur as faults slip, it is important to understand what processes influence throw rate variability on normal faults to be able to predict seismic hazards in extensional terranes. Furthermore, the rate of normal fault growth directly controls rift physiography, sediment erosion, dispersal and deposition, and the distribution and stratigraphic architecture of syn-rift reservoirs. Instrumental (e.g. geodetic) data may constrain the co-seismic movement on, or relatively short-term (i.e. $<10^3$) throw rate history of, normal faults, whereas palaeoearthquake data may provide important information on medium-term (i.e. 10^3-10^5 years) rates. Constraining longer-term (i.e. $>10^6$ Myr) variations typically requires the use of seismic reflection data, although their application may be problematic because of poor seismic resolution and the absence of, or poor age constraints on, coeval growth strata. In this study I use 3D seismic reflection and borehole data to constrain the growth and (minimum) long-term throw rate variability on a gravity-driven, salt-detached normal fault (Middle-to-Late Jurassic) in the South Viking Graben, offshore Norway, and to assess the impact of throw rate variability on the thickness and character of syn-rift reservoirs. I recognise five kinematic phases: (i) Phase 1 (early Callovian) - fault initiation and a phase of moderate fault throw rates (0.06 mm yr^{-1}); (ii) Phase 2 (early Callovian-to-end Callovian) - fault inactivity, during which time the fault was buried by sediment; (iii) Phase 3 (early Oxfordian-to-late Oxfordian) - fault reactivation and a phase of moderate throw rates (up to 0.03 mm yr^{-1}); (iv) Phase 4 (late Oxfordian-to-end Oxfordian) – a marked increase in throw rate (up to 0.27 mm yr^{-1}); and (v) Phase 5 (early Kimmeridgian-to-middle Volgian) – a decline in throw rate (0.03 mm yr^{-1}) and eventual death of the fault. These rates are comparable to those observed on other gravity-driven normal faults, with the variability in this example apparently kinematically coupled with the growth history of the thick-skinned normal fault system bounding the western margin of the basin. Fluctuations

in sediment accumulation rate and loading may have also influenced throw rate variability. Shallow marine reservoirs deposited when throw rate was relatively low (Phase 1) increase in thickness but do not change in facies across the fault, principally because sediment accumulation rate outpaced fault throw rate. In contrast, deep-marine turbidite reservoirs, despite being characterised by relatively high sediment accumulation rates, were deposited when the throw rate was relatively high (Phase 4), thus are only preserved in the fault hangingwall. Variations in throw and sediment accumulation rate may therefore act as dual controls on the thickness and distribution of syn-rift reservoirs in salt-influenced rift basins.

INTRODUCTION

The rate of growth of normal faults is important, influencing earthquake behaviour and thus hazard determination in extensional settings (e.g. Nicol et al., 2005a,b; Mouslopoulou et al., 2009, 2012). Furthermore, rift physiography and thus sediment erosion, dispersal and deposition are controlled by the style and rates of normal fault growth (Gawthorpe and Leeder, 2000), which may in turn impact the distribution, stratigraphic architecture and quality of syn-rift reservoirs. Throw or displacement rate variability on normal faults may reflect: (i) relatively local mechanical interactions between segments forming part of a kinematically coherent array (e.g. Nicol et al., 1997; Cowie, 1998; Cowie et al., 2000; Gawthorpe and Leeder, 2000); (ii) regional variations in the magnitude of far-field plate tectonic forces and regional strain rates, perhaps related to variations in the rate and style of tectonic processes occurring at the genetically related plate boundary (e.g. Nicol et al., 2005a,b; Mouslopoulou et al., 2009, 2012); and (iii) variations in sediment accumulation rate and loading, which may be of particular importance in thin-skinned, gravity-driven systems developing above mobile substrates (e.g. Lowrie, 1986; Cartwright et al., 1998; Brothers et al., 2013; Smith et al., 2013). Field-based analysis of throw or displacement rate variability on active or ancient (i.e. inactive) faults typically utilise: (i) geodetic analysis; (ii) cosmogenic isotope analysis of exposed fault scarps (e.g. Schlagenhauf et al., 2010); and (iii) dating of offset stratigraphic markers exposed in natural or man-made trenches crossing active or recently active normal faults; and (iv) historical palaeoearthquake records (see discussion by Nicol et al., 2005a,b). These analytical approaches yield important data on short-term (i.e. co-seismic up to 10^5 years) displacement (or throw) rate variations although this may not be representative of the longer term (i.e. $>10^6$ year) behaviour (Fig. 1) (e.g. Nicol et al. 2005a,b; Mouslopoulou et al., 2009, 2012). Seismic reflection data can be applied to constrain long-term displacement (or throw) rates on surface-breaking (growth) faults although its application can be problematic due to: (i) poor seismic resolution, which hampers our ability to map faults and related growth strata that record fault kinematics; (ii) the absence of growth strata due to uplift and erosion of the fault footwall, a situation common on large (i.e. km-scale displacement or throw) faults; and (iii) poor age constraints on growth strata.

The Gudrun Fault, located in the South Viking Graben, offshore Norway (Fig. 2) provides an exceptional opportunity to constrain the long-term (>10^6 year) throw rate history of a salt-detached normal fault. The general geometry, and Middle-to-Late Jurassic kinematic and tectono-stratigraphic development of the Gudrun Fault are described by Jackson & Larsen (2009), Kieft et al. (2010) and Jackson et al. (2011). What remains unknown is how throw rate varied on the fault through time, and what controlled such variations; resolving these issues forms the focus of this paper. Adjacent to the Gudrun Fault, seismic data are of sufficient quality to map the fault and associated growth strata and, due to relatively high sediment accumulation rates, syn-kinematic growth strata are almost fully preserved in the fault hangingwall and footwall of the fault. Biostratigraphic data constrain the age of growth strata on both sides of the fault, allowing me to determine its throw rate. I demonstrate that the throw rate history of the Gudrun Fault was highly variable. I then argue that this variability is kinematically coupled to throw rate variations on the thick-skinned, basement-involved normal fault bounding the western margin of the half-graben, which controlled the rate of hangingwall rotation and extension of the suprasalt cover. Fluctuations in sedimentation rate and loading in this gravity-driven extensional system may also have played a role in controlling throw rate variations. Irrespective of the precise mechanisms controlling variations in its throw rate, these variations influenced the distribution, thickness and quality of shallow- and deep-marine syn-rift reservoirs.

GEOLOGICAL SETTING

The study area is located in the South Viking Graben, offshore Norway (Fig. 2). The South Viking Graben is a c. 40 km wide, gently (5˚) westwards-tilted half-graben, bound on its western margin by a large displacement (up to 5 km), N- to NNE-striking, E-dipping normal fault system (the Graben Boundary Fault Zone). The South Viking Graben formed in response to Permo-Triassic and Middle-to-Late Jurassic rifting, although the geometry of the basin is dominated by structures associated with the latter rift event.

During the Late Permian, the South Viking Graben was located along the northern margin of the Northern Permian Salt Basin, where it formed a NE-trending, fault-bounded embayment. An evaporite-dominated succession (the Zechstein Supergroup) was deposited in the South Viking Graben at this time (Fig. 3) (e.g. Glennie, 1990; Ziegler, 1990; Hodgson et al., 1992; Glennie, 1995); this unit strongly influencing the structural style of the Middle-to-Late Jurassic rift event and the Late Jurassic-to-Early Cretaceous inversion event (Pegrum & Ljones, 1984; Thomas & Coward, 1996; Jackson and Larsen, 2008, 2009). During the Triassic, a broadly tabular succession of lacustrine mudstones (Smith Bank Formation) and fluvial sandstones (Skagerrak Formation) were deposited above the salt (Fig. 3) (e.g. Fischer & Mudge, 1998).

Lower Jurassic strata are absent in the South Viking Graben due to syn-depositional growth of the Mid-North Sea Dome (Ziegler, 1990; Underhill and Partington, 1993, 1994). During the Middle Jurassic, the Mid-North Sea Dome deflated and the Graben Boundary Fault Zone reactivated, resulting in rapid subsidence of the South Viking Graben (Harris and Fowler, 1987; Ziegler, 1990; Cockings et al., 1992; Coward, 1995; Thomas and Coward, 1996). Fault-controlled subsidence, coupled with a eustatic rise in sea-level, resulted in deposition of an upward-fining, Middle-to-Upper Jurassic succession. Coastal-plain (Sleipner Formation) and shallow marine (Hugin Formation) sandstone, mudstone and coal pass upward into siltstone-dominated shelf deposits (Heather Formation) and mudstone-dominated deep marine deposits, which locally contain thick (>250 m) turbidite sandstone that form the main reservoirs in the Gudrun field (Draupne Formation) (Figs 3 and 4) (Harris and Fowler, 1987; Cockings et al., 1992; Fraser et al., 2003; Hampson et al., 2009; Kieft et al., 2010; Jackson et al., 2011; Hoth et al., this volume). Overall, these changes in depositional system type and sediment supply direction resulted in: (i) an initial decrease in sediment supply and accumulation rate linked to southwards backstepping of the 'Brent' delta (i.e. the upward stratigraphic transition from the Sleipner to Hugin to Heather Formation); and following this (ii) a subsequent upward increase in sediment supply and accumulation rate linked to the main phase of rifting, degradation of the Utsira High and the related influx of deep-water sandstones.

Hangingwall tilting during Middle-to-Late Jurassic rifting resulted in the formation of salt-detached normal faults in the Triassic-Middle Jurassic cover overlying Zechstein salt (Figs 2B, 5 and 6) (Thomas and Coward, 1995; Jackson and Larsen, 2009). The Gudrun Fault, which forms the focus of this study, is perhaps the best-imaged salt-detached normal fault in the South Viking Graben. Jackson and Larsen (2009) demonstrate that the Gudrun Fault initiated in the late Middle Jurassic (Late Callovian), broadly coeval with the initiation of activity on the Graben Boundary Fault Zone, and became inactive during the Late Jurassic (Early Kimmeridgian).

The South Viking Graben was inverted during the latest Jurassic (late Early Volgian) and the majority of rift-related faults became inactive (Jackson and Larsen, 2008). Inversion led to development of low-relief anticlinal buckle folds in the hangingwalls of many of the Upper Jurassic rift-related normal faults (Fig. 6A) (e.g. Pegrum and Ljones, 1984; Cherry, 1993; Knott et al., 1993; 1995; Thomas and Coward, 1996; Knott, 2001; Branter, 2003; Brehm, 2003; Fletcher, 2003a,b; Jackson and Larsen, 2008). Jackson and Larsen (2008) demonstrate that the hangingwall of the Gudrun Fault was folded but that the fault itself was not reverse reactivated. This is an important observation, indicating that the original syn-extensional geometry and throw variations on the Gudrun Fault are preserved.

DATASET

The study area is covered by a 3D seismic reflection dataset, with an inline (NE-SW) and crossline (NW-SE) spacing of 12.5 m and record length of 5.5 seconds. The seismic data are displayed with reverse polarity (SEG European convention) so that a downward increase in acoustic impedance is represented by a trough or ‘soft’ event (black reflection on the profiles presented here) and a downward decrease in acoustic impedance is represented by a peak or ‘hard’ event (white reflection on the profiles presented here) (Fig. 6). The vertical scale of the seismic data is in two-way time (TWT), but measurements taken from the data (e.g. fault throw, thickness of stratigraphic packages) were converted to metres based on velocity data taken from boreholes 15/3-1S and 15/3-7 (Figs 2 and 4). The vertical seismic resolution in the interval of interest is 30-40 m (Jackson et al., 2011) and seismic data quality is generally good-to-excellent, although it is poor beneath the Zechstein salt.

Two wells containing core, electrical log (e.g. gamma-ray = GR; density = RHOB; velocity=DT) and biostratigraphic data were utilised in this study (15/3-1S, 15/3-7; Figs 4, 5A and 6A). 15/3-1S penetrates the hangingwall of the Gudrun Fault, whereas 15/3-7 penetrates the footwall, both being located near the centre of the fault where throw is highest (Jackson and Larsen, 2009). Core data from these two wells and three nearby wells (15/3-3, 3-4 and 3-5) are described in detail by Kieft et al. (2010) (Hugin Formation) and Jackson et al. (2011) (Draupne Formation); these data provide a direct calibration of the penetrated sedimentary facies and allow us to infer likely facies in uncored wells (or uncored intervals of wells). Thirteen key stratal surfaces, constrained by biostratigraphically defined surfaces tied to the ammonite-based, North Sea-wide scheme of Partington et al. (1993), are identified in and correlated between wells, allowing an age-constrained seismic-stratigraphic framework to be constructed for growth strata preserved adjacent to the Gudrun Fault (Figs 3 and 4). Five seismic reflections were mapped: (i) top Rotliegend Group; (ii) top Zechstein Supergroup; (iii) top Sleipner Formation; (iv) top Hugin Formation; and (v) top Draupne Formation; Fig. 3A). Further details on the data and methods used to subdivide the syn-rift succession into biostratigraphically defined, sub-seismic stratal units are provided below.

GEOMETRY AND ORIGIN OF THE GUDRUN FAULT

The Gudrun Fault is 15 km long, strikes NE-SW, is planar in cross-section and dips steeply (66-80°) to the north-west (Figs 5 and 6A). The fault detaches downwards onto pre-rift

Zechstein salt and terminates upward into the syn-rift Draupne Formation (Late Oxfordian-Middle Volgian) (Fig. 6A). Maximum throw (c. 615 m) occurs at the centre of the Gudrun Fault (as measured at the base of the Hugin Formation; Fig. 3), decreasing along strike to the fault tips (Fig. 5A). Gentle folding in the hangingwall of the Gudrun Fault (Fig. 6A) is related to minor post-rift inversion (Thomas and Coward, 1996; Jackson and Larsen, 2008, 2009).

Jackson and Larsen (2009) note that; (i) the footwall to the Gudrun Fault displays no systematic along-strike variations in uplift; (ii) syn-rift strata are broadly tabular in the footwall of the fault (Fig. 6C); (iii) the hangingwall defines a broad syncline whose axis is located near the centre of the fault (Fig. 5A); and (iv) syn-rift strata thicken along-strike into the centre of this syncline (Fig. 6B). Based on these geometric and seismic-stratigraphic characteristics, I interpret that syn-rift activity on the Gudrun Fault was dominated by hangingwall subsidence with only minor if any, complimentary footwall uplift; these features are characteristic of thin-skinned, gravity-driven growth faults forming above salt or shale detachments (e.g. Fazli Khani and Back, 2012).

THROW RATE VARIABILITY ON THE GUDRUN FAULT

In this section I investigate temporal variations in throw rate on the Gudrun Fault, using the terms ‘low-resolution kinematic analysis’ and ‘high-resolution kinematic analysis’ in a relative sense. ‘Low-resolution’ refers to the kinematic history derived from seismic-stratigraphic analysis of the growth strata adjacent to the fault (i.e. the straight dashed line in Fig 1). This can include analysis of stratigraphic thickness (i.e. isochron or isopach) maps generated by seismic mapping of ‘upper’ 3rd-order (c. 5 x 10^6 years) sequences or offset of key seismic reflections across faults. ‘High-resolution’ refers to the kinematic history derived from analysis of borehole data (i.e. the curved and ‘stair step-like’ lines in Fig. 1). This includes analysis of the magnitude of offset of sub-seismic stratigraphic surfaces across the fault, and thickness variations in the ‘lower’ 3rd-order (i.e. 1-2 x 10^6 years) sub-seismic sequences they bound.

Using growth strata to constrain the kinematics of normal fault growth requires that the fault is blanketed by syn-kinematic sediment during its growth (i.e. the basin was overfilled; Childs et al., 2003). If this is the case and if local, depositional system-related variations in sediment accumulation rate can be discounted (a reasonable assumption in this case given the relatively small size of the fault relative to the scale of the coeval depositional systems), it is likely that the observed thickness variations are the direct result of fault-driven changes in accommodation. Data from the Gudrun Fault indicate that the syn-rift succession is preserved in and thickens from the footwall to the hangingwall of the fault (Figs 4 and 6), suggesting that sediment accumulation rate was greater than fault throw rate during Middle-to-Late Jurassic rifting.

Low-resolution kinematic analysis

Thomas and Coward (1996) use regional 2D seismic reflection and borehole data to demonstrate that the Gudrun Fault (and several other faults on the hangingwall of the South Viking Graben) was active during the Middle-to-Late Jurassic rift event (cf. Jackson and Larsen, 2008). Jackson and Larsen (2009) come to broadly the same conclusion using 3D seismic reflection and borehole data, arguing there were four key kinematic phases during growth of the Gudrun Fault: (i) early Callovian (164.2-162 Ma) - initiation of faulting and early fault growth; (ii) middle to late Callovian (162-159.5 Ma) - cessation of faulting; (iii) late Callovian and early Oxfordian (159.5-155 Ma) - reactivation and lateral and vertical propagation of the fault; and (iv) late Kimmeridgian (c. 152 Ma) - death of the fault. Thickening of the entire early Callovian-to-middle Volgian syn-rift succession (i.e. Hugin Formation to intra-Draupne Formation; Fig. 6A) across the Gudrun Fault indicates the structure was, apart from a ca. 2.5 Myr period of inactivity in the middle-to-late Callovian (Jackson and Larsen, 2009; Jackson et al., 2011), active for 12.2 Myr. Based on a maximum throw of c. 615 m at the fault centre (measured at the base of the Hugin Formation) and the age constraints placed on the top (152 Ma) and base (164.2 Ma) of the syn-rift succession, I calculate a long-term throw rate of 0.05 mm yr^{-1} for the Gudrun Fault (red line on Fig. 7C).

Backstripping of age-constrained seismic horizons (e.g. Chapman and Meneilly, 1991; Petersen et al., 1992; Childs et al., 2003) permits a higher-fidelity analysis of the growth history and throw rate variability on the Gudrun Fault. For this analysis I use base Hugin Formation (end Bathonian; 164.2 Ma), top Hugin Formation (early Callovian; 162.2 Ma), top Heather Formation (early late Oxfordian; 156 Ma), and top SU4a (end Oxfordian; 154.2 Ma). This analysis yields the following throw rates; (i) early Callovian (Hugin Formation; sub-unit 1) = 0.05 mm yr^{-1}; (ii) early Callovian to late Oxfordian (Heather Formation; sub-units 2-5) = 0.01 mm yr^{-1}; (iii) late Oxfordian (SU4a; sub-units 6-7 = 0.17 mm yr^{-1}; and (iv) early Kimmeridgian (lower SU4b; sub-unit 8 = 0.05 mm yr^{-1}) (blue line in Fig. 7C)). Note that the last calculation assumes that the base of SU4b, which broadly defines the death of the Gudrun Fault, is approximately 152 Myr. Although this refines the throw rate history of the Gudrun Fault (cf. curves on Fig. 1), I demonstrate below that this rate is still not representative of the entire 12.2 Myr growth history of the fault.

High-resolution kinematic analysis

To investigate the high-resolution growth history of the Gudrun Fault I use borehole data from the footwall (15/3-7) and the hangingwall (15/3-1S) of the fault to constrain the age and thickness of associated growth strata. Three main lithostratigraphic units are defined in the syn-rift succession: the Hugin (SU2), Heather (SU3) and Draupne (SU4) formations ('SU' nomenclature after Jackson and Larsen, 2009 and Jackson et al., 2011; Figs 3 and 4). Twelve sub-units are identified in the syn-rift succession, bounded by 13 biostratigraphically defined key stratal surfaces (Figs 3 and 4). Each sub-unit is 26-360 m thick and represents a 0.5-2.9 Myr time interval. I use expansion indices (EI) analysis (see Thorsen, 1963) to describe changes in stratal thickness across the Gudrun Fault. Borehole data also constrain across-fault changes in sedimentary facies, highlighting the impact syn-depositional faulting had on accommodation, water depth and sediment dispersal (see Kieft et al., 2010 and Jackson et al., 2011 for detailed, core- and wireline log-based descriptions of Middle and Upper Jurassic facies types and their distribution, respectively). It should be noted that the throw rate values given below are calculated for compacted thicknesses of growth strata; these values should therefore be considered as minimum values (i.e. decompaction would yield thicker sequences of growth strata deposited per unit time, which would thus result in an increase in the absolute throw rate; see also Taylor et al., 2008). As I show below, the Gudrun Fault experienced five main kinematic phases (cf. the four phases identified by Jackson and Larsen, 2009, which was derived from a largely seismic-based kinematic analysis), defined by deposition of specific syn-rift sub-units; Phase 1 (early Callovian) = sub-unit 1; Phase 2 (early Callovian-to-end Callovian) = sub-units 2 and 3; Phase 3 (early Oxfordian-to-late Oxfordian) = sub-units 4 and 5; Phase 4 (late Oxfordian) = sub-units 6 and 7; Phase 5 (early Kimmeridgian-to-middle Volgian) = sub-units 8-12. Throw rates (black line in Fig. 7C) and characteristic across-fault thickness and facies changes associated with each phase are described below.

Phase 1 (early Callovian). Phase 1 corresponds to deposition of marginal marine deposits of the Hugin Formation (sub-unit 1; Figs 3, 4 and 7) (Cockings et al., 1992; Kieft et al., 2010). Constraining the thickness of the Hugin Formation in the hangingwall of the Gudrun Fault is not directly possible because borehole 15/3-1S) does not penetrate the entire formation (Fig. 4), However, Jackson and Larsen (2009) measure the seismically defined thickness of the Hugin Formation in two-way time (TWT) and use borehole-derived velocity information to convert this value to metres; based on this approach they estimate that the formation is c. 360 m thick in the hangingwall of the Gudrun Fault. Based on wireline log signatures, calibrated to observations in a cored succession in the adjacent footwall well, Kieft et al. (2010) interpret that the upper few hundred metres of the Hugin Formation comprises backbarrier heteroliths and tidal inlet sandstone (15/3-7; Fig. 4). The Hugin Formation is almost fully penetrated in the footwall of the Gudrun Fault (15/3-7) and again, by using borehole-derived velocity information to convert a seismically defined thickness of the formation from TWT to metres, Jackson and Larsen (2009) estimate the unit is c. 225 m thick. This value is similar to that encountered in borehole 15/3-3 (235 m), which is drilled only 4.5 km along strike and which fully penetrates the Hugin Formation. These data indicate that Hugin Formation thickens across the fault and has an expansion index of 1.5 (Figs 4 and 7). Jackson and Larsen (2009) and Kieft et al. (2010) demonstrate that the Hugin Formation comprises four parasequences and, more specifically, that the upper two parasequences (units 'C' and 'D' of Jackson and Larsen, 2009), which are the only ones fully penetrated in the hangingwall of the Gudrun Fault (15/3-1S) and which are also fully penetrated in the footwall (15/3-7), have expansion indices significantly greater than inferred for the unit as a whole (i.e. 2.7 for Unit C and 3.1 for Unit D, compared to 1.5 for the whole Hugin Formation; Fig. 4). This observation indicates that across-fault thickening is not distributed evenly in the Hugin Formation and that fault-driven differential subsidence was most pronounced during the latter stages of deposition of this unit.

During Phase 1 (2.3 Myr), based on my estimates of its hangingwall and footwall thickness, the sediment accumulation rate during deposition of the Hugin Formation was relatively high (0.13 mm yr^{-1}) and the throw rate on the Gudrun Fault was relatively low (c. 0.06 mm yr^{-1}) (Fig. 7) (cf. long-term displacement rates of Mouslopoulou et al., 2009; their Table 1). The Hugin Formation is therefore preserved in the hangingwall and footwall of the Gudrun Fault although, due to a lack of core data, it is more difficult to make a detailed assessment of the impact syn-depositional faulting had on across-fault facies partitioning. The apparent stratigraphic variability that is observed in intervals fully penetrated in the hangingwall (upper part of B, C and D; 15/3-1S) and footwall (upper part of A, B-D; 15/3-7) may reflect fault-controlled variations in water depth or tidal energy but it may, however, reflect the inherent depositional variability of the tidally influenced system represented by the Hugin Formation (Kieft et al., 2010). What is clear is that, because sediment accumulation rate was high relative to fault throw rate, overall thickening of at least the upper part of the Hugin Formation across the Gudrun Fault was accommodated by across-fault thickening of individual parasequences rather than by the addition of parasequences in the hangingwall (parasequences C and D; Fig. 4) (see Hodgetts et al., 2001). I speculate that, due to high sediment accumulation rates, the fault had no or only limited topographic expression and was not expressed as a scarp at the depositional surface. Because of this, faulting may not have influenced sediment dispersal, although syn-depositional motion on the structure clearly resulted in preservation of an expanded hangingwall succession in at least the upper part Hugin Formation.

Phase 2 (early Callovian-to-end Callovian). Phase 2 correlates with deposition of the lower part of the shelf-deposited Heather Formation, which is defined by moderate GR log values in both the hangingwall and footwall (sub-units 2 and 3; Figs 3, 4 and 7). Sub-unit 2 thickens slightly across the fault (21.24 m in the footwall to 31 m in the hangingwall; EI=1.5), whereas sub-unit 3 thins slightly across the fault (35.35 m in the footwall to 26 m in the hangingwall;

EI=0.8); taken together, these units are essentially the same thickness on either side of the fault (i.e. 56.59 m in the footwall to 57 m in the hangingwall; EI=1.2) (Figs 4 and 7).

During Phase 2 (2.8 Myr), the sediment accumulation rate was relatively low (average of 0.02 and 0.03 mm yr^{-1} for sub-units 2 and 3 respectively) and the Gudrun Fault was essentially inactive (Fig. 7) (Jackson and Larsen, 2009; Jackson et al., 2011). Although core data are lacking and because the Callovian shelf was widespread and sand-poor (Fraser et al., 2003), the uniform GR log signature strongly suggests the Heather Formation did not change facies across the fault change (Fig. 4).

Phase 3 (early Oxfordian-to-late Oxfordian). Phase 3 corresponds to deposition of the upper part of the shelf-deposited Heather Formation, which, like the lower part, is defined by moderate GR log values in both the hangingwall and footwall (sub-units 4 and 5; Figs 3, 4 and 7). In contrast to sub-units 2 and 3, which were of broadly equal thickness on either side of the Gudrun Fault, sub-unit 4 thickens significantly across the fault (37.6 m in the footwall and 119 m in the hangingwall; EI=3.2). Across-fault thickening of sub-unit 5 also occurs but is subtler (Figs 4 and 7) (30.4 m in the footwall to 37.5 m in the hangingwall; EI=1.2).

During Phase 3 (2.6 Myr), the sediment accumulation rate was relatively low (0.03 and 0.07 mm yr^{-1} for sub-units 4 and 5 respectively) as was the Gudrun Fault throw rate (c. 0.03 and 0.01 mm yr^{-1} during deposition of sub-units 4 and 5 respectively; cf. long-term displacement rates of Mouslopoulou et al., 2009; their Table 1), being lower than during Phase 1 but higher than during Phase 2 (Fig. 7). Despite the sedimentation accumulation rate being relatively low, it was still higher than the throw rate (at least during deposition of sub-unit 4). Despite lacking core data, based on the uniform GR log signature and the widespread, sand-poor nature of the Early Oxfordian shelf (Fraser et al., 2003), I infer the upper part of the Heather Formation did not change facies across the fault and that simply an expanded hangingwall succession was preserved (Fig. 4).

Phase 4 (late Oxfordian-to-end Oxfordian). Phase 4 correlates with deposition of the lower part of the deep-marine Draupne Formation (sub-units 6 and 7; Figs 3, 4 and 7). Sub-units 6 (43 m in the footwall to 136 m in the hangingwall; EI=3.2) and 7 (13 m in the footwall to 230 m in the hangingwall; EI=17.7) display major across-fault thickening, the latter being the most pronounced across-fault thickening observed in the entire syn-rift succession (Figs 4 and 7).

The striking across-fault thickness change described above is accompanied by a correspondingly significant across-fault change in sedimentary facies. In sub-units 6 and 7, which document 3.3 Myr of deposition during Phase 4, the hangingwall succession contains thick-bedded turbidite sandstone whereas the footwall succession is mudstone-dominated (Fig. 4) (see detailed sedimentological description by Jackson et al., 2011). These across-fault changes in thickness and facies correspond to the highest throw rates observed on the Gudrun Fault (c. 0.09 and 0.27 mm yr^{-1} during deposition of sub-units 6 and 7 respectively; Fig. 7), although these rates are still very low when compared to the long-term rates compiled by Mouslopoulou et al. (2009) (their Table 1). Jackson et al. (2011) interpret that, at this time, the hangingwall basin was intermittently underfilled, and that a fault scarp-related bathymetric step triggered a hydraulic jump in the deep-water turbidity currents, which resulted in preferential deposition of turbidite sandstone immediately downdip of the Gudrun Fault and filling of the hangingwall (see Fig. 12A in Jackson et al. 2011). The sediment accumulation rate during deposition of sub-unit 6 is relatively high (0.06 and 0.068 mm yr^{-1} for sub-units 6 and 7 respectively) compared to those in the underlying units; the sediment accumulation rate in the hangingwall of the Gudrun Fault during deposition of sub-unit 7 is the highest observed in the entire syn-rift succession (0.128 mm yr^{-1}) (Fig. 7).

Phase 5 (early Kimmeridgian-to-middle Volgian). Phase 5 corresponds to deposition of the upper part of the deep-marine Draupne Formation (sub-units 8-12; Figs 3, 4 and 7). Sub-unit 8 also thickens significantly across the fault (4 m in the footwall to 39 m in the hangingwall; EI=9.8), whereas sub-unit 9, which was deposited during and slightly after the death of the Gudrun Fault (Jackson and Larsen, 2009; Jackson et al., 2011), displays moderately striking across-fault thickening (118 m in the footwall to 174 m in the hangingwall; EI=2.6) (Figs 4 and 7). Sub-units 10-12 are not offset by the Gudrun Fault, thus the very modest thickness variations in these units (EI=<1.5) are demonstrably not fault related; I instead interpret these short length-scale (<2 km) variations in thickness and facies to reflect spatial variability in sediment dispersal, incision and deposition in this deep-marine slope setting (Figs 4 and 7) (Jackson et al., 2011).

During the early part of Phase 5 (8.9 Myr), the throw rate on the Gudrun Fault, immediately prior to its death, was relatively low (0.03 mm yr^{-1}) (Fig. 7) (cf. long-term displacement rates of Mouslopoulou et al., 2009; their Table 1). The sediment accumulation rate of deep-marine slope mudstone in the hangingwall of the Gudrun Fault was also relatively low (c. 0.03 mm yr^{-1}) (sub-unit 8 and lowermost part of sub-unit 9; Figs 4 and 7). In the footwall, this interval is represented by an unconformity and it is not known if deposition was restricted to the fault hangingwall, or whether mudstone deposited in the footwall was later eroded during turbidity current-driven sediment bypass (see Jackson et al., 2011). Sub-unit 9 comprises a 70-175 m thick turbidite sandstone body that extends across the upper tip of the Gudrun Fault into the footwall and hangingwall of the fault (Fig. 4). Deposition of this turbidite-dominated succession was associated with a very high sediment accumulation rate (hangingwall rate of 0.12 mm yr^{-1}), comparable to that characterising earlier major sand influxes during deposition of sub-unit 7 (i.e. 0.13 mm yr^{-1}) (Fig. 7). North-eastwards thickening of sub-unit 9 may reflect syn-depositional subsidence of the Gudrun Fault hangingwall, induced by compaction of an underlying, relatively fine-grained succession in this location compared to the thinner succession in the footwall (Fig. 4). Sub-units 10-12 are dominated by slope mudstone, with relatively thin (up to 25 m) turbidite sandstone bodies occurring at multiple stratigraphic levels (Fig. 4). Sediment accumulation rates during deposition of these mudstone-dominated sub-units were relatively modest (hangingwall rates of 0.02, 0.01 and 0.04 mm yr^{-1} for sub-units 10, 11 and 12, respectively; Fig. 7).

DISCUSSION

Controls on throw rate variability during thin-skinned extension in the South Viking Graben

Five kinematic phases characterise the growth of the Gudrun Fault during Middle-to-Late Jurassic rifting; (i) Phase 1 - fault initiation and a phase of moderate fault throw rates (early Callovian); (ii) Phase 2 - fault inactivity, during which time the fault was buried by sediment (early Callovian-to-end Callovian); (iii) Phase 3 - fault reactivation and a phase of moderate throw rates (early Oxfordian-to-late Oxfordian); (iv) Phase 4 – a marked increase in throw rate (late Oxfordian-to-end Oxfordian); and (v) Phase 5 – a decline in throw rate and eventual death of the fault (early Kimmeridgian-to-middle Volgian). Given this growth history, the key question arising from this study is what drove variations in throw rate on the Gudrun Fault?. Nucleation of the fault during the Callovian can be attributed to the initiation of activity on the Graben Boundary Fault Zone bounding the western margin of the South Viking Graben (Fig. 2), and consequential westwards rotation of the hangingwall. Thick-skinned faulting initiated gravity-gliding and extension of the Triassic-to-lower Middle Jurassic suprasalt cover above Zechstein salt (Thomas and Coward, 1996; Jackson and Larsen, 2008, 2009; Jackson et al., 2011). It is therefore appealing to link variations in throw rate on the Gudrun Fault to variations in displacement (or throw) rate on the Graben Boundary Fault Zone; in this sense, throw rate variations on the Gudrun Fault reflect regional changes in the tectonic boundary conditions driving extension (cf. Mouslopoulou et al., 2009). Most authors agree that after the initial Callovian period of thick-skinned faulting and hangingwall rotation, the Graben Boundary Fault Zone was very active and experienced high displacement rates during the Middle-to-Late Oxfordian (Cockings et al., 1992; Cherry, 1993; McClure and Brown, 1992; Fletcher, 2003a,b; Fraser et al., 2003), which is broadly coincident with the main period of accelerated subsidence on the Gudrun Fault (Phase 4; Figs 7 and 8). High displacement rates on the Graben Boundary Fault Zone and rapid subsidence of the South Viking Graben would have driven rapid tilting of the hangingwall dipslope, and the Zechstein salt and its cover; this would have continued into and through the Kimmeridgian (early Phase 5; Figs 7 and 8). The decay and eventual death of the Gudrun Fault occurred during the late Kimmeridgian (c. 152 Ma), broadly coincident with waning activity on the Graben Boundary Fault Zone, which began in the latest Kimmeridgian and continued until the Volgian (Fig. 8) (Jackson and Larsen, 2008; Jackson et al., 2011). In detail, however, death of the Gudrun Fault appears to have occurred slightly earlier than the waning and eventual death of the Graben Boundary Fault Zone (Fig. 8), suggesting that another process or set of processes might have been responsible for the cessation of activity on the hangingwall structure. Jackson and Larsen (2009) suggest that death of the Gudrun Fault occurred due to thinning and perhaps local welding of Zechstein salt beneath its hangingwall, with strain migrating upslope onto the newly formed Brynhild Fault.

In addition to broadly correlating to periods of enhanced activity on the Graben Boundary Fault Zone, I also note that variations in throw rate on the Gudrun Fault are positively correlated with fluctuations in sediment accumulation rate (Fig. 7). Generally speaking, periods of high sediment accumulation rate during deposition of the marginal-marine Hugin Formation (sub-unit 1) and turbidite-dominated, lower part of Draupne Formation (sub-unit 7) correlate with periods of high-to-very high relative throw rate (Phases 1 and 7; Fig. 7). In contrast, during deposition of the shelfal Heather Formation (sub-units 2-5) and slope mudstone-dominated, upper part of the Draupne Formation (sub-unit 8), when sediment accumulation rates were low, throw rates were correspondingly low-to-moderate (Phases 2-3 and 5; Fig. 7). More specifically, a progressive increase in sediment accumulation rate during deposition of sub-units 4 through to 7 is associated with a progressive increase in throw rate (Fig. 7). Given this temporal relationship between sediment accumulation rate and fault throw rate, and the fact that the Gudrun Fault forms part of a salt-detached gravity-driven system, I speculate that fluctuating rates of sediment accumulation and detachment loading in the hangingwall of the Gudrun Fault drove variable throw rates (cf. Lowrie, 1986; Cartwright et al., 1998). Thus far-field tectonic processes (i.e. initiation and variable rates of displacement on the Graben Boundary Fault Zone; see above) and local variability in the rate of sediment accumulation could have had a dual control on throw rate variability on the Gudrun Fault.

Controls on throw rate variability on other salt-detached normal faults

There are few detailed descriptions of displacement, slip or throw rate variability on thin-skinned faults above mobile intra-stratal detachments (e.g. salt, overpressured shale). Most work has focused on thick-skinned or basement-involved ‘tectonic’ faults, formed due to continental extension driven by plate motions, because of the earthquake hazard they pose (e.g. Nicol et al., 2005b). Using 3D seismic and borehole data from the onshore Niger Delta, Pochat et al. (2009) constrain throw rate variability on a shale-detached normal fault, identifying two kinematic phases: (i) an early phase of at least 9 Myr characterised by relatively high throw rates (0.09–0.12 mm yr^{-1}); and (ii) a late phase of c. 3 Myr, immediately prior to death of the fault, characterised by relatively low throw rates (0.01–0.015 mm yr^{-1}). For much, but not all of its history, the fault of Pochat et al. (2009) was characterised by higher rates of offset than the Gudrun Fault (Fig. 7). Without additional data on the geological context of the Niger Delta growth fault (e.g. nature and thickness of the detachment, spatial and kinematic relationship to other thin-skinned structures, temporal fluctuations in sediment accumulation rate), the reasons for this difference are unclear. The higher displacement rate on the Niger Delta fault may be attributed to the overall gravitational potential of the system of which it forms a part; i.e. seaward (south-westward) tilting of the west African margin and shale detachment, and consequent extension and normal faulting of the cover, may have been more rapid in the Niger Delta example than the genetically similar process that drove salt-detached extension in the South Viking Graben. Higher sediment accumulation rates in the Niger Delta, which was obviously fed by a much larger drainage system than that feeding the Jurassic South Viking Graben, may also have contributed to higher slip rates. In the case that the rates of tilting and, more unlikely, the sediment accumulation in both locations were similar, a lower viscosity (shale) detachment in the Niger Delta example may have resulted in more rapid overburden extension and higher fault displacement rates. An alternative interpretation is that the Niger Delta fault was kinematically isolated from other structures and thus slipped faster than the Gudrun Fault which was, at least during part of its growth, sharing strain with a nearby structure (i.e. the Brynhild Fault; Jackson and Larsen, 2009; Jackson et al., 2011).

Using 3D seismic reflection and borehole data, Childs et al. (2003) document throw rates of 0.07-0.22 mm yr^{-1} for salt-detached growth faults on the Gulf Coast, southern US. Analysing the same types of faults, using similar data, and in the same general setting, Alexander and Flemings (1995) constrain slip rates of 0.4-2.3 mm yr^{-1}. In detail, slip rates initially increase (from 0.4 to 2.3 mm yr^{-1}) in response to delta progradation and an increasing sediment accumulation rate (c. 1-3 mm yr^{-1}), before decreasing (to 0.5 mm yr^{-1}) in response to delta topset aggradation and a stable to slightly decreasing sediment accumulation rate (from 2.3 to 1.6 mm yr^{-1}). These observations indicate that, in general, sediment loading likely drove slip rate variations; more specifically, however, variations in sediment loading likely drove variations in the rate of salt evacuation from below a subsiding minibasin and hence overburden deformation. As discussed above, variations in sediment accumulation rate and substrate loading may have played a role in slip rates variations on the Gudrun Fault.

Dutton and Trudgill (2009) use 3D seismic reflection data from offshore Angola to constrain throw rate variations on Oligocene-to-Recent, salt-detached normal faults that are of similar geometry and genesis, if not scale, to those documented in the South Viking Graben. They argue that a Pliocene (c. 5 Ma) extensional pulse was triggered by increased sediment input and thus substrate loading, driven by progradation of the Congo Fan. Fault kinematics are thus directly linked to variations in sediment accumulation and loading, in a similar way to that suggested for the Gudrun Fault and the structures studied on the Gulf Coast (Alexander and Flemings, 1995; Childs et al., 2003). After the fault system initiated, throw rate varied from 0.02-0.16 mm yr^{-1}, which is within the range documented here and from other thin-skinned extensional provinces. Moreover, on the fault for which they have most data (i.e. their 'rearward segment'), Dutton and Trudgill (2009) demonstrate that throw rate decreased with time (from 0.16 to 0.04 mm yr^{-1} over 5 Myr), which they attribute to a combination of increasing mechanical and thus kinematic interactions between adjacent faults, and progressive thinning and eventual welding of salt, which reduced shear within the detachment and thus led to a decrease in the rate of cover extension and faulting.

A range of factors may thus control slip or throw rates on gravity-driven faults. Certainly, the difference described from the five examples above appear real and not simply a function of data quality; i.e. 3D seismic reflection datasets are of comparable quality, well data are present in the immediate footwall and hangingwall of the studied structures, and the temporal resolution of the mapped seismic horizons is broadly similar, except for the Gulf Coast case study where the temporal resolution is <1 Myr (Alexander and Flemings, 1995).

Impact of throw rate variability on reservoir development

Throw rate variations on the Gudrun Fault impacted the thicknesses and facies of syn-rift reservoirs (Kieft et al., 2010; Jackson et al., 2011). In general, when the sediment accumulation rate was high relative to fault throw rate, syn-rift reservoirs changed thickness but not facies across the fault. For example, in the Hugin Formation, an across-fault increase in bulk thickness was accommodated by thickening of individual parasequences rather than by the addition of extra parasequences in the hangingwall of the fault. Increased parasequence thickness may not, however, correlate to an increase in reservoir net-to-gross (N:G), which is instead controlled by whether across-fault thickening accommodating expansion of the lower, poorer-quality or upper, higher-reservoir quality part of the parasequence. In summary, when throw (or displacement) rate is relatively low or at least low relative to sediment accumulation rate, reservoirs may be deposited on both sides of a normal fault, but it may be of varying quality and undoubtedly thickness.

During Late Oxfordian deposition of the Draupne Formation, when throw rates were high relative to the rate of sediment accumulation, intra-slope relief was created, resulting in the formation of an intra-slope depocentre that was bound on its updip margin by the Gudrun Fault. This intra-slope bathymetric step defined by the Gudrun Fault forced sand-laden turbidity currents to undergo a hydraulic jump and deposit their load. Turbidite sandstone reservoirs are thus only present in the hangingwall of the Gudrun Fault, the footwall instead being an area of sediment bypass (see also Jackson et al., 2011; Stevenson et al., in press). In summary, when throw (or displacement) rate is relatively high or at least high relative to sediment accumulation rate, reservoirs may only be deposited in the fault hangingwall.

CONCLUSIONS

3D seismic reflection and borehole data were used to constrain throw rates and growth history of a salt-detached normal fault in the South Viking Graben, offshore Norway. The principal results of this study are:

1. The Gudrun Fault is characterised by five kinematic phases: (i) Phase 1 (early Callovian) - fault initiation and a phase of moderate fault throw rates (0.06 mm yr^{-1}); (ii) Phase 2 (early Callovian-to-end Callovian) - fault inactivity, during which time the fault was buried by sediment; (iii) Phase 3 (early Oxfordian-to-late Oxfordian) - fault reactivation and a phase of moderate throw rates (up to 0.03 mm yr^{-1}); (iv) Phase 4 (late Oxfordian-to-end Oxfordian) – a marked increase in throw rate (up to 0.27 mm yr^{-1}); and (v) Phase 5 (early Kimmeridgian-to-middle Volgian) – a decline in throw rate (0.03 mm yr^{-1}) and eventual death of the fault.
2. As first suggested by Jackson and Larsen (2009), the thin-skinned Gudrun Fault initiated at approximately the same time as the thick-skinned fault system bounding the basin margin with periods of faster throw rate on the two being temporally coupled. These observations suggest that the two may be kinematically coupled, with activity on the thick-skinned system controlling the rate of hangingwall tilting, cover extension and therefore salt-detached normal faulting.
3. Throw rate appears positively correlated to sediment accumulation rate, suggesting that fluctuations in sediment loading driven by regional fluctuations in supply may have also driven throw rate variations on this gravity-driven fault.
4. Throw rates on the Gudrun Fault are comparable to those observed on other ancient and active, salt- and overpressured shale-detached gravity-driven normal faults and are broadly similar to those measured from thick-skinned faults developed in active extensional terranes. Throw rate variability in both types of systems likely reflect interactions between faults forming part of a kinematically coherent array, with detachment characteristics and rate of sub-detachment tilting being particularly important in gravity-driven systems.
5. Shallow marine reservoirs deposited when the throw rate was relatively low (Phase 1) increase in thickness but perhaps not change in facies across the fault, principally

because sediment accumulation rate outpaced fault throw rate. In contrast, deep-marine turbidite reservoirs, despite being characterised by relatively high sediment accumulation rates, were deposited when the throw rate was relatively high (Phase 4), thus are only preserved in the fault hangingwall. Throw (or displacement) rate variability and sediment accumulation rate thus act as dual controls on the thickness and distribution of syn-rift reservoirs in both thin- and thick-skinned extensional settings.

6. 3D seismic reflection data and borehole data can be used to constrain the long-term (i.e. >10^6 Myr) throw (or displacement) rates and growth histories of ancient and active normal faults. Successful application of these data requires that: (i) growth strata are preserved adjacent to the fault; (ii) seismic data quality is sufficient to accurately map the faults and growth strata, the latter recording fault kinematics; and (iii) borehole data constrain the age of growth strata. With sufficient data quantity and quality, the approach outlined here could be applied at the array scale to many fault segments and systems.

ACKNOWLEDGMENTS

I thank Eirik Larsen, Anna-Elise Tjemsland, Colin Turner, Karla Kane, Rachel Kieft, Gary Hampson, Anna-Sofia Gregerson, Unni Stalsberg Sjursen, Elisebeth Bjerkebeck and Helge Sognnes for discussions during the course of this study. Statoil ASA are thanked for providing financial support and data during the initial part of this study. Memoir Editor Colin Turner is thanked for providing encouragement.

REFERENCES

Alexander, L.L., and Flemings, P.B., 1995, Geologic evolution of a Pliocene-Pleistocene salt-withdrawal minibasin: Eugene Island Block 330, offshore Louisiana. AAPG bulletin, 79, 1737-1756.

Branter, S.R.F., 2003, The East Brae Field, Blocks 16/03a, 16/03b, UK North Sea, in J. Gluyas and H.M. Hichens, eds., United Kingdom Oil and Gas Fields: Commemorative Millennium Volume, Geological Society, London, Memoir, 20, 191-197.

Brehm, J.A., 2003, The North Brae and Beinn Fields, Block 16/7a, UK North Sea, in J. Gluyas and H.M. Hichens, eds., United Kingdom Oil and Gas Fields, Commemorative Millennium Volume, Geological Society, London, Memoir, 20, 199-209.

Brothers, D.S., Luttrell, K.M., Chaytor, J.D., 2013, Sea-level-induced seismicity and submarine landslide occurrence. Geology, 41, 979-982.

Cartwright, J., Bouroullec, R., James, D., Johnson, H., 1998, Polycyclic motion history of some Gulf Coast growth faults from high-resolution displacement analysis. Geology, 26, 819-822.

Chapman, T.J., and Meneilly, A.W., 1991, The displacement patterns associated with a reverse reactivated normal fault in A. Roberts, G. Yielding, B. Freeman, eds., Geometry of normal faults: Geological Society, London, Special Publication, 56, 183-191.

Cherry, S.T.J., 1993, The interaction of structure and sedimentary process controlling deposition of the Upper Jurassic Brae Formation Conglomerate, Block 16/17, North Sea, in J.R. Parker, ed., Petroleum Geology of northwest Europe: Proceedings of the 4th conference, Geological Society, London, 387-400.

Childs, C., Nicol, A., Walsh, J.J. and Watterson, J. 2003. The growth and propagation of synsedimentary faults. Journal of Structural Geology 25, 633-648.

Cockings, J.H., Kessler II, L.G., Mazza, T.A. and Riley, L.A., 1992, Bathonian to mid-Oxfordian sequence stratigraphy of the South Viking Graben, North Sea in R.F.P. Hardman, ed., Exploration Britain; Geological Insights for the Next Decade: Geological Society, London, Special Publication, 67, 65-105.

Coward, M.P., 1995, Structural and tectonic setting of the Permo-Triassic basins of northwest Europe in S.A.R. Boldy, ed., Permian and Triassic rifting in Northwest Europe: Geological Society, London, Special Publication, 91, 7-39.

Cowie, P.A., 1998, A healing–reloading feedback control on the growth rate of seismogenic faults. Journal of Structural Geology, 20, 1075–1087.

Cowie, P.A., Gupta, S. and Dawers, N.H., 2000, Implications of fault array evolution for syn rift depocentre development: insights from a numerical fault growth model. Basin Research, 12, 241–262.

Dutton, D.M., and Trudgill, B.D., 2009, Four-dimensional analysis of the Sembo relay system, offshore Angola: Implications for fault growth in salt-detached settings. AAPG Bulletin, 93, 763-794.

Fazli Khani, H. and Back, S., 2012, Temporal and lateral variation in the development of growth faults and growth strata in the western Niger Delta, Nigeria. AAPG Bulletin, 96, 595-614.

Fischer, M.J. and Mudge, D.C., 1998, Triassic in K.W. Glennie, ed., Petroleum Geology of the North Sea; Basin concepts and recent advances: Blackwell, Oxford, 212-244.

Fletcher, K.J., 2003a The Central Brae Field, Blocks 16/07a, 16/07b, UK North Sea. In: United Kingdom Oil and Gas Fields, Commemorative Millennium Volume (Ed. by J. Gluyas & H.M. Hichens), Geological Society, London, Memoir, 20, 183-190.

Fletcher, K.J., 2003b, The South Brae Field, Blocks 16/07a, 16/07b, UK North Sea, in J. Gluyas and H.M. Hichens, eds., United Kingdom Oil and Gas Fields, Commemorative Millennium Volume, Geological Society, London, Memoir, 20, 211-221.

Fraser, S.I., Robinson, A.M., Johnson, H.D., Underhill, J.R., Kadolsky, D.G.A., Connell, R., Johannessen, P., and Ravnås, R., 2003, Upper Jurassic in D. Evans, C. Graham, A. Armour and P. Bathurst, eds., The Millennium Atlas: petroleum geology of the central and northern North Sea: The Geological Society of London, 157-189.

Gawthorpe, R.L. and Leeder, M.R., 2000, Tectono-sedimentary evolution of active extensional basins. Basin Research, 12, 195–218.

Glennie, K.W., 1990, Outline of the North Sea history and structural framework in K.W. Glennie Introduction to the petroleum geology of the North Sea 2nd edition: Blackwell Scientific Publications, Oxford, 25-62.

Glennie, K.W., 1995, Permian and Triassic Rifting in Northwest Europe in S.A.R. Boldy, ed., Permian and Triassic rifting in Northwest Europe: Geological Society, London, Special Publication, 91, 1-5.

Hampson, G.J., Sixsmith, P.J., Kieft, R.L., Jackson, C.A-L. and Johnson, H.D., 2009, Quantitative analysis of net-transgressive shoreline trajectories and stratigraphic architectures: mid-to-late Jurassic of the North Sea rift basin. Basin Research, 21, 528-558.

Harris, J.P. and Fowler, R.M., 1987, Enhanced prosperity of the Mid-Late Jurassic sediments of the South Viking Graben, northern North Sea in J. Brooks and K.W. Glennie, eds., Petroleum Geology of northwest Europe: Proceedings of the 3th conference: Geological Society, London, 879-898.

Hodgetts D, Imber, J., Childs, C. and Flint, S., 2001, Sequence stratigraphic responses to shoreline-perpendicular growth faulting in shallow marine reservoirs of the Champion Field, offshore Brunei Darussalam, South China Sea. AAPG Bulletin, 85, 433-457.

Hodgson, N.A., Farnsworth, J., and Fraser, A.J., 1992, Salt-related tectonics, sedimentation and hydrocarbon plays in the Central Graben, North Sea, UKCS in R.F.P. Hardman, ed., Exploration Britain: Insights for the Next Decade: Geological Society of London Special Publication, 67, 31-63.

Jackson, C.A-L. and Larsen, E., 2008, Temporal constraints on basin inversion provided by 3D seismic and well data: a case study from the South Viking Graben, offshore Norway. Basin Research, 20, 397-417.

Jackson, C.A-L. and Larsen, E., 2009, Temporal and spatial development of a gravity-driven normal fault array: Middle–Upper Jurassic, South Viking Graben, northern North Sea: Journal of Structural Geology, 31, 388 – 402.

Jackson, C.A-L., Larsen, E., Hanslien, S. and Tjemsland, A-E., 2011, Controls on synrift turbidite deposition on the hanging wall of the South Viking Graben, North Sea rift system, offshore Norway. AAPG Bulletin, 95, 1557-1587.

Kieft, R.L., Jackson, C.A-L., Hampson, G.J. and Larsen, E., 2010, Sedimentology and sequence stratigraphy of the Hugin Formation, Quadrant 15, Norwegian sector, South Viking Graben, London, Petroleum Geology: From Mature Basins to New Frontiers. Geological Society of London, 157-176.

Cohen, K.M., Finney, S.C., Gibbard, P.L. and Fan, J.-X., 2013, The ICS International Chronostratigraphic Chart. Episodes, 36, 199-204.

Knott, S.D., 2001, Gravity-driven crustal shortening in failed rifts. Journal of the Geological Society, 158, 193-196.

Knott, S.D., Burchell, M.T., Jolley, E.J. and Fraser, A.J., 1993, Mesozoic to Cenozoic plate reconstructions of the North Atlantic and hydrocarbon plays of the Atlantic margins. In: Petroleum Geology of northwest Europe: Proceedings of the 4th conference (Ed. by J.R. Parker), Geological Society, London, 953-974.

Knott, S.D., Beach, A., Welbon, A. I. and Brockbank, P.J., 1995, Basin inversion in the Gulf of Suez. In: Basin Inversion (Ed. By J.G. Buchanan & P.G. Buchanan), Geological Society, London, Special Publication, 88, 59-82.

Lowrie, A., 1986, Model for fine-scale movements associated with climate and sea level changes along Louisiana shelfbreak growth faults: Gulf Coast Association of Geological Societies Transactions, 36, 497–509.

McClure, N.M., and Brown, A.A., 1992, A subtle Upper Jurassic submarine fan trap in the South Viking Graben, United Kingdom, North Sea in M. Halbouty, ed., Giant Oil and Gas Fields of the Decade (1978-1988): American Association of Petroleum Geologists Memoir, 54, 307–322.

Mouslopoulou, V., Walsh, J.J. and Nicol, A., 2009, Fault displacement rates on a range of timescales. Earth and Planetary Science Letters, 278, 186-197.

Mouslopoulou, V., Nicol, A., Walsh, J.J., Begg, J.G., Townsend, D.B. and Hristopulos, D.T., 2012, Fault-slip accumulation in an active rift over thousands to millions of years and the importance of paleoearthquake sampling. Journal of Structural Geology, 36, 71-81.

Nicol, A., Walsh, J.J., Watterson, J. and Underhill, J.R., 1997, Displacement rates of normal faults. Nature, 390, 157-159.

Nicol, A., Walsh, J., Berryman, K. and Nodder, S., 2005a, Growth of a normal fault by the accumulation of slip over millions of years. Journal of Structural Geology, 27, 327-342.

Nicol, A., Walsh, J.J., Manzocchi, T. and Morewood, N., 2005b, Displacement rate and average earthquake recurrence intervals on normal faults. Journal of Structural Geology, 27, 541-551.

Partington, M.A., Copestake, P., Mitchener, B.C. and Underhill, J.R., 1993, Biostratigraphic calibration of genetic stratigraphic sequences in the Jurassic–lowermost Cretaceous (Hettangian to Ryazanian) of the North Sea and adjacent areas. *In*: Geological Society, London, Petroleum Geology Conference series, vol. 4, pp. 371-386. Geological Society of London.

Petersen, K., Clausen, O.R. and Korstgård, J.A., 1992, Evolution of a salt-related listric growth fault near the D-1 well, block 5605, Danish North Sea. Journal of Structural Geology, 14, 565-577.

Pegrum, R.M. and Ljones, T.E., 1984, 15/9 Gamma gas field offshore Norway, new trap type for the North Sea basin with regional structural implications. AAPG Bulletin, 68, 874-902.

Pochat, S., Castelltort, S., Choblet, G. and Van Den Driessche, J., 2009, High-resolution record of tectonic and sedimentary processes in growth strata. Marine and Petroleum Geology, 26, 1350-1364.

Schlagenhauf, A., Gaudemer, Y., Benedetti, L., Manighetti, I., Palumbo, L., Schimmelpfennig, I., Finkel, R. and Pou, K., 2010, Using in-situ Chlorine 36 cosmonuclide to recover past earthquake histories on limestone normal fault scarps: A reappraisal of methodology and interpretations. Geophysical Journal International, 182, 36-72.

Smith, D.E., Harrison, S., Jordan, J.T., 2013, Sea level rise and submarine mass failures on open continental margins. Quaternary Science Reviews, 82, 93-103.

Stevenson, C.J., Jackson, C.A-L., Hodgson, D.M., Hubbard, S.M. and Eggenhuisen, J.T., 2015, Deep-water sediment bypass. Journal of Sedimentary Research, 85, 1058-1081.

Thomas, D.W. and Coward, M.P., 1995, Late Jurassic-Early Cretaceous inversion of the northern East Shetland Basin, northern North Sea in J.G. Buchanan and P.G. Buchanan, eds., Basin Inversion: Geological Society, London, Special Publication, 88, 275-306.

Thomas, D.W. and Coward, M.P., 1996, Mesozoic regional tectonics and South Viking Graben formation; evidence for localized thin-skinned detachments during rift development and inversion. Marine and Petroleum Geology, 13, 149-177.

Thorsen, C. E., 1963, Age of growth faulting in south-east Louisiana: Gulf Coast Association of Geological Societies Transactions, 13, 103–110.

Underhill, J.R. and Partington, M.A., 1993, Jurassic thermal doming and deflation: the sequence-stratigraphic evidence in J.R. Parker, ed., Petroleum Geology of northwest Europe: Proceedings of the 4th conference: Geological Society, London, 337-345.

Underhill, J.R. and Partington, M.A., 1994, Use of genetic sequence stratigraphy in determining a regional tectonic control on the "Mid-Cimmerian Unconformity": implications for North Sea basin development in P. Weimer, and H.W. Posamentier, eds., Siliciclastic Sequence Stratigraphy: AAPG Memoir, 58, 449-484.

Ziegler, P.A., 1990, Tectonic and paleogeographic development of the North Sea rift system in D. Blundell and A.D. Gibbs, eds., Tectonic Evolution of the North Sea Rifts, Oxford Clarendon Press, 1-36.

FIGURE CAPTIONS

Figure 1. Schematic diagram illustrating fault-slip accumulation over instrumental (days to years), palaeoearthquake (e.g. <25 Kyr) and geological (e.g. >300 Kyr to several million years) timescales. Numbered steps in the palaeoearthquake data represent large ground-surface rupturing earthquakes, whereas steps in the day-to-year long data represent small-sized instrumentally recorded earthquakes that may not have ruptured the Earth's surface. Depending on the temporal window of analysis and method, the fault may appear to accumulate displacement at uniform (i.e. long-term window), approximately uniform (i.e. medium-term window) or variable (i.e. short-term window) rates. Data resolution increases with decreasing timescales (modified from Mouslopoulou et al., 2009, 2012).

Figure 2. (A) Simplified map illustrating the key structural elements of the South Viking Graben. For clarity, only the main extensional faults related to the Late Jurassic rift event are shown. The inset map shows the geographic location of the study area. The locations of the study area shown in Fig. 5 and the geoseismic section shown in Fig. 2B are indicated. Modified from Thomas and Coward (1996). (B) Simplified geoseismic section across the South Viking Graben illustrating the main structural features and their spatial relationships. 15/3-1S and 15/3-7 are key boreholes used to constrain the age and composition of faulted strata and, therefore, displacement rate variations on the Gudrun Fault (GF). See (A) for location of section.

Figure 3. (A) Simplified stratigraphic column illustrating the upper Palaeozoic to Mesozoic stratigraphy of the South Viking Graben. Mapped seismic horizons are labelled and the structural and/or stratigraphic significance of the various units is indicated (i.e. column marked 'Tectono-stratigraphic significance'). 'J'-surface nomenclature is from Underhill and Partington (1993, 1994). Stratigraphic ornament applies to the geoseismic profiles shown in Fig. 6. (B) Details for the late Middle and Upper Jurassic stages offset by the Gudrun Fault. The identified kinematic phases are indicated in the right-hand column. "J" nomenclature for the maximum flooding surfaces (MFS) corresponds to that established by Partington et al. (1993) and stratigraphic ages are consistent with those published by the Cohen et al. (2013). The stratigraphic position and approximate ages of seismic reflection events mapped in this study are indicated, as are the mapped stratal units (SU). Other key stratal surfaces constrained by biostratigraphic data and bounding sub-seismic sub-units are indicated. Lwr = lower; Mid = middle; Upr = upper; E = early; M = middle; L = late.

Figure 4. Stratigraphic correlation between 15/3-1S and 15/3-7 located in the hangingwall and footwall of the Gudrun Fault respectively. The identified kinematic phases, stratal units (SU) and sub-units are indicated, in addition to the biostratigraphically defined key stratal surfaces constraining the correlation (see also Jackson et al., 2011). A-D in SU2 refer to informally defined, intra-Hugin Formation parasequences defined by Jackson and Larsen (2009) (see also Kieft et al., 2010). Facies for the Hugin Formation (Kieft et al., 2010) and the Heather and Draupne formations (Jackson et al., 2011) are directly constrained by core data (red boxes) or, in uncored intervals, inferred from wireline responses calibrated to cored intervals.

Figure 5. (A) Time-structure and (B) simplified sketch maps showing the main structures observed at the top of SU2 (i.e. top Hugin Formation; see Fig. 3). These maps illustrate the main thin-skinned, gravity-driven Upper Jurassic rift-related faults (including the Gudrun Fault) and associated folds. The locations of wells used in this study are shown. BFC = Brynhild fault central; BFS = Brynhild fault south; GF = Gudrun fault (see Jackson and Larsen, 2008, 2009). Locations of seismic profiles shown in Fig. 6 are indicated.

Figure 6. (A) Fault-normal seismic profile and corresponding geoseismic section across the central part of the Gudrun Fault. (B) Fault-parallel seismic profile and corresponding geoseismic section in the immediate hangingwall of the Gudrun Fault. (C) Fault-parallel seismic profile and corresponding geoseismic section in the immediate footwall of the Gudrun Fault. Key to stratigraphic ornament is shown in Fig. 3. Abbreviations for the key structures are the same as in Fig. 5. Locations of profiles are shown in Fig. 5.

Figure 7. (A) Expansion Index (EI), (B) sedimentation rate and (C) cumulative throw data for the Gudrun Fault derived from boreholes 15/3-1S and 15/3-7 (see Fig. 4). Relatively short-term displacement rates (i.e. <2 Myr) are indicated in bold italic text adjacent to the black line in (C). The red line indicates the time-averaged, long-term (i.e. 12.2 Myr) throw rate (mm/yr) for the Gudrun Fault based on the bulk thickness of the syn-rift succession and the maximum fault offset; the blue line indicates the throw rate for specific periods (i.e. 2-7 Myr duration) of the growth of the Gudrun Fault based on throw backstripping of seismic horizons (cf. Childs et al., 2003). See text for full discussion.

Figure 8. Wheeler-style diagram illustrating overall geometry of the South Viking Graben and the bulk composition and age relationships between the main syn-rift units. The timing of activity on thick- (i.e. Graben Boundary Fault Zone or 'GBFZ') and thin-skinned (Gudrun and Brynhild faults) components of the extensional array is indicated, in addition to periods of accelerated displacement (intervals defined by thicker black bars on fault markers). See text for full discussion. "J" nomenclature for the maximum flooding surfaces (MFS) corresponds to that established by Partington et al. (1993) and stratigraphic ages are consistent with those published by the International Commission on Stratigraphy (2014). Modified from McClure and Brown (1992), Turner et al. (in review) and Turner and Connell (in review).

Fig. 1

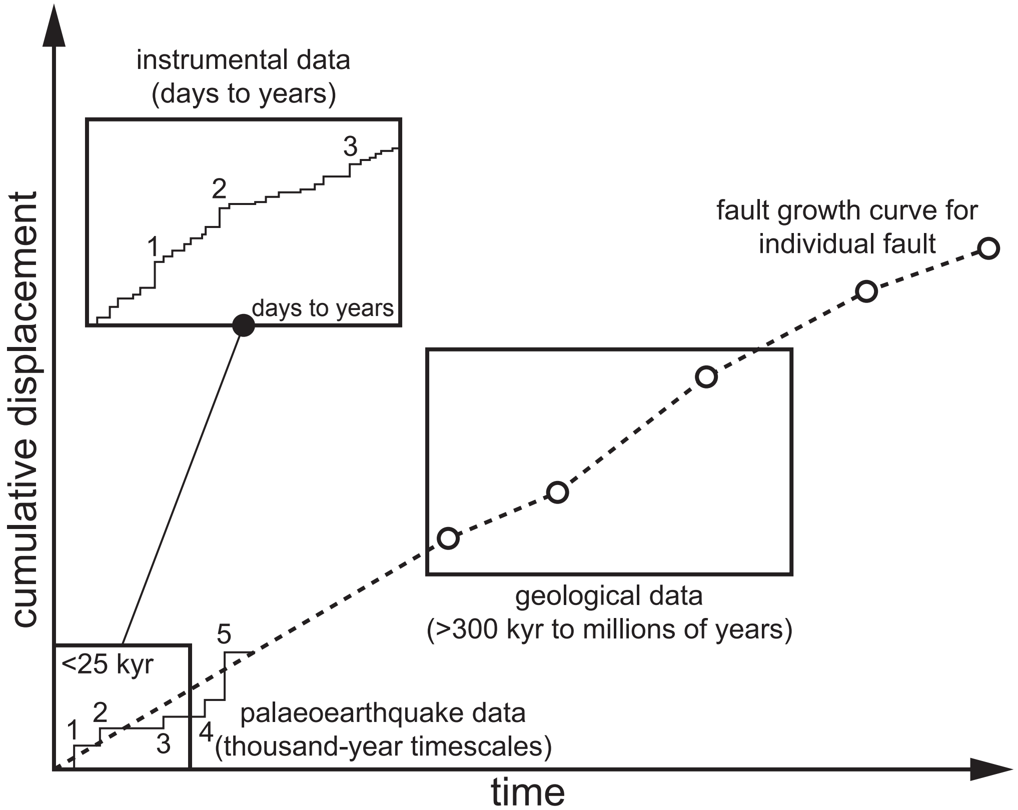
instrumental data
(days to years)
1
2
3
days to years
fault growth curve for
individual fault
geological data
(>300 kyr to millions of years)
<25 kyr
1
2
3
4
5
palaeoearthquake data
(thousand-year timescales)
cumulative displacement
time

Fig. 2

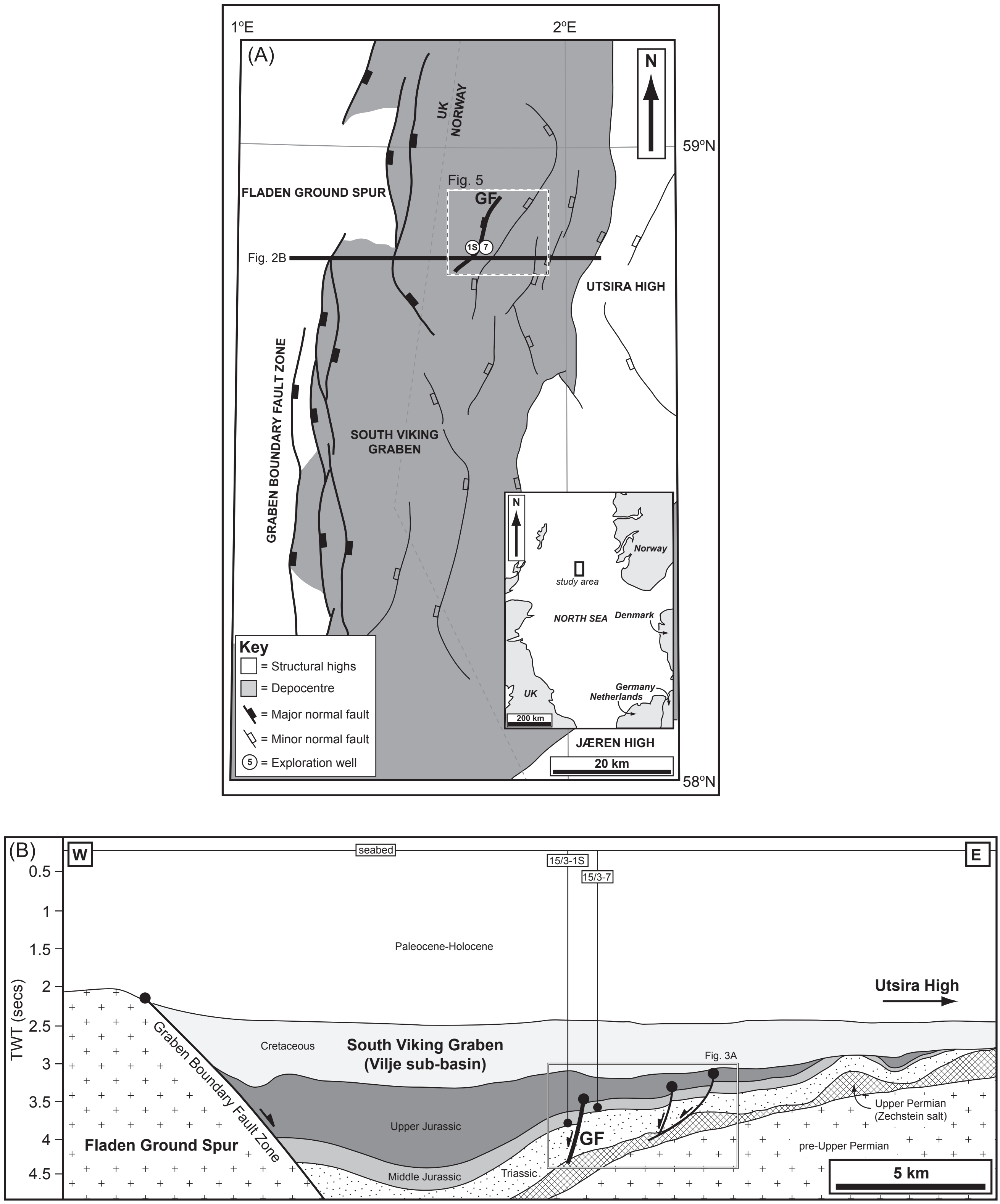

(A)
1ºE
2ºE
59ºN
58ºN
N
UK
NORWAY
Fig. 5
GF
FLADEN GROUND SPUR
Fig. 2B
1S
7
UTSIRA HIGH
GRABEN BOUNDARY FAULT ZONE
SOUTH VIKING GRABEN
Norway
study area
NORTH SEA
Denmark
UK
Germany
Netherlands
200 km
JÆREN HIGH
20 km
Key
= Structural highs
= Depocentre
= Major normal fault
= Minor normal fault
5 = Exploration well
(B)
W
E
seabed
15/3-1S
15/3-7
TWT (secs)
0.5
1
1.5
2
2.5
3
3.5
4
4.5
Paleocene-Holocene
Utsira High
Cretaceous
South Viking Graben
(Vilje sub-basin)
Fig. 3A
Graben Boundary Fault Zone
Upper Jurassic
GF
Upper Permian
(Zechstein salt)
Fladen Ground Spur
pre-Upper Permian
Middle Jurassic
Triassic
5 km

Fig. 3

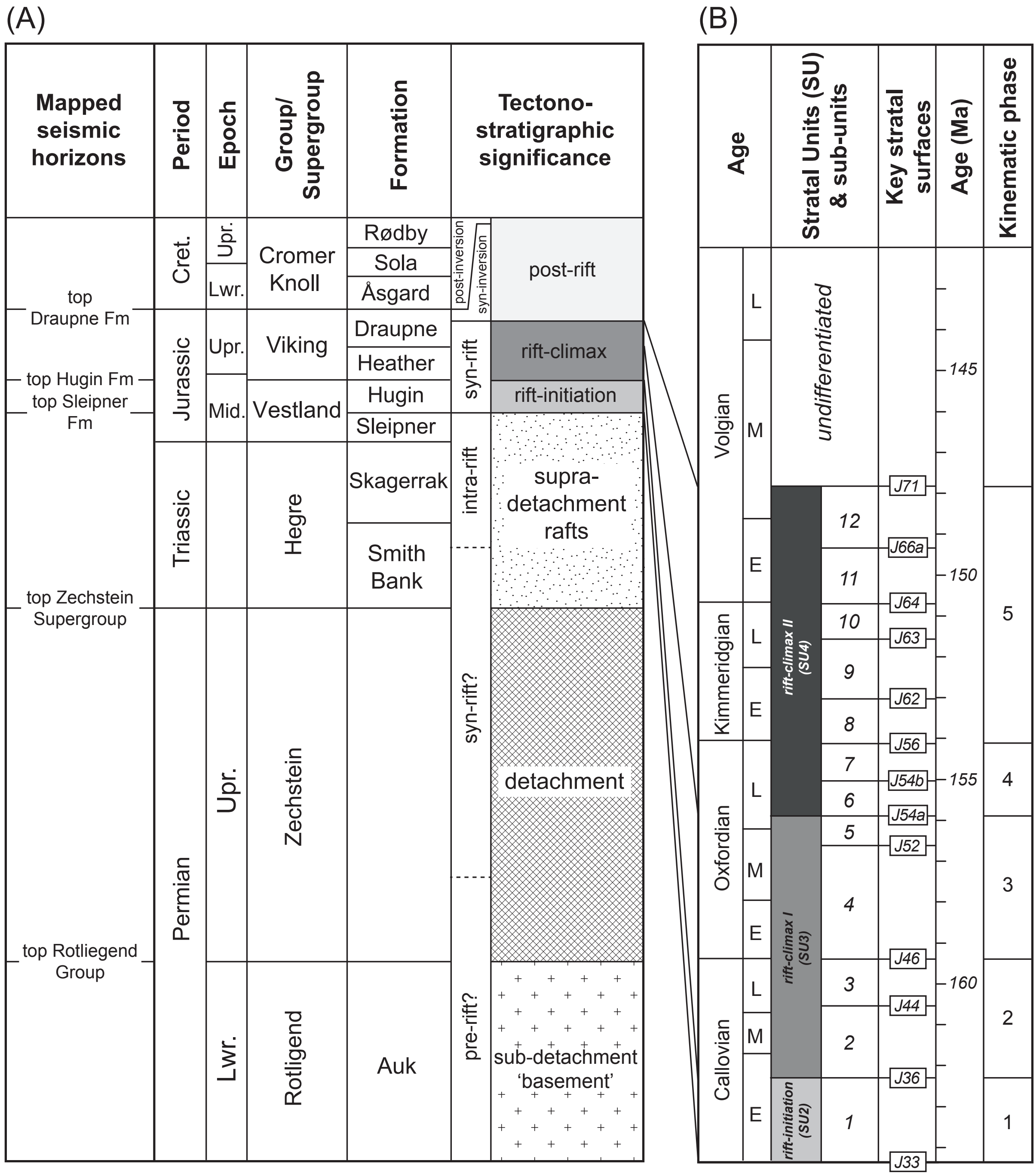
(A)
Mapped seismic horizons
Period
Epoch
Group/ Supergroup
Formation
Tectono-stratigraphic significance
top Draupne Fm
top Hugin Fm
top Sleipner Fm
top Zechstein Supergroup
top Rotliegend Group
Cret.
Upr.
Lwr.
Jurassic
Upr.
Mid.
Triassic
Permian
Upr.
Lwr.
Cromer Knoll
Viking
Vestland
Hegre
Zechstein
Rotligend
Rødby
Sola
Åsgard
Draupne
Heather
Hugin
Sleipner
Skagerrak
Smith Bank
Auk
post-inversion
syn-inversion
post-rift
syn-rift
rift-climax
rift-initiation
intra-rift
supra-detachment rafts
syn-rift?
detachment
pre-rift?
sub-detachment 'basement'
(B)
Age
Stratal Units (SU) & sub-units
Key stratal surfaces
Age (Ma)
Kinematic phase
Volgian
Kimmeridgian
Oxfordian
Callovian
L
M
E
undifferentiated
rift-climax II (SU4)
rift-climax I (SU3)
rift-initiation (SU2)
12
11
10
9
8
7
6
5
4
3
2
1
J71
J66a
J64
J63
J62
J56
J54b
J54a
J52
J46
J44
J36
J33
145
150
155
160
5
4
3
2
1

Fig. 4

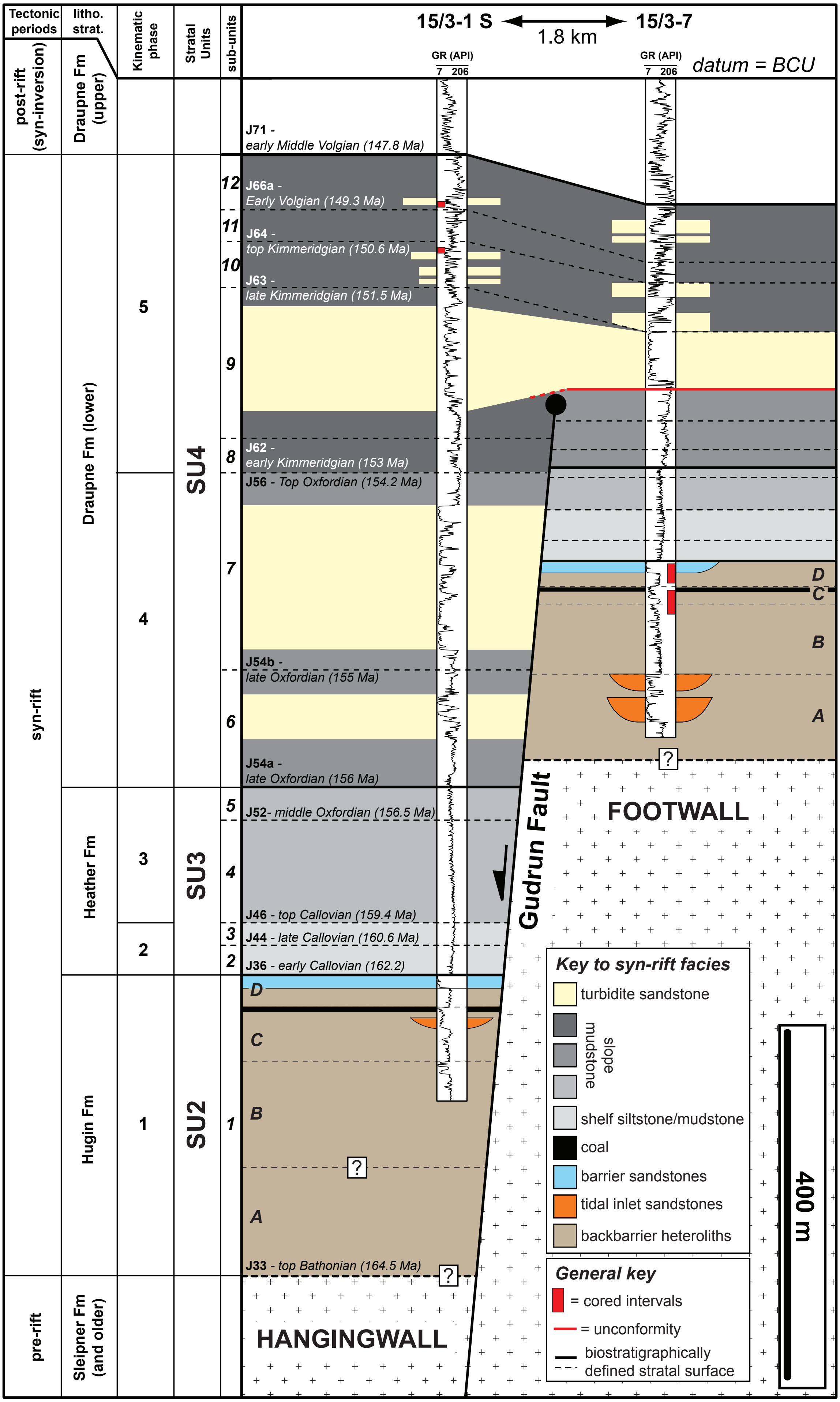

Tectonic periods
litho. strat.
Kinematic phase
Stratal Units
sub-units
15/3-1 S
1.8 km
15/3-7
GR (API)
7 206
datum = BCU
post-rift (syn-inversion)
syn-rift
pre-rift
Draupne Fm (upper)
Draupne Fm (lower)
Heather Fm
Hugin Fm
Sleipner Fm (and older)
SU4
SU3
SU2
J71 - early Middle Volgian (147.8 Ma)
J66a - Early Volgian (149.3 Ma)
J64 - top Kimmeridgian (150.6 Ma)
J63 - late Kimmeridgian (151.5 Ma)
J62 - early Kimmeridgian (153 Ma)
J56 - Top Oxfordian (154.2 Ma)
J54b - late Oxfordian (155 Ma)
J54a - late Oxfordian (156 Ma)
J52- middle Oxfordian (156.5 Ma)
J46 - top Callovian (159.4 Ma)
J44 - late Callovian (160.6 Ma)
J36 - early Callovian (162.2)
J33 - top Bathonian (164.5 Ma)
Gudrun Fault
FOOTWALL
HANGINGWALL
Key to syn-rift facies
turbidite sandstone
slope mudstone
shelf siltstone/mudstone
coal
barrier sandstones
tidal inlet sandstones
backbarrier heteroliths
General key
= cored intervals
= unconformity
biostratigraphically defined stratal surface
400 m

Fig. 5

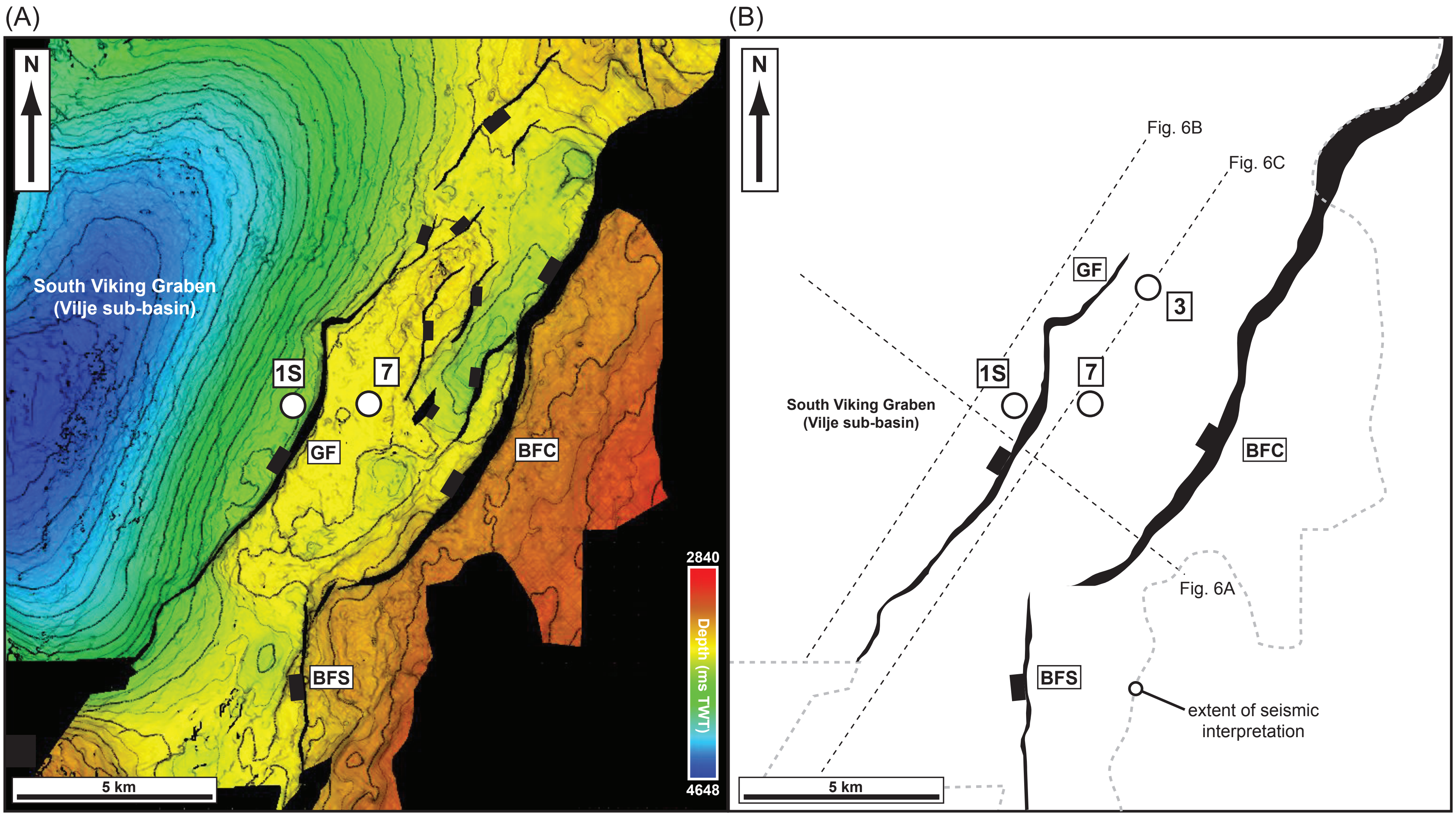

(A)
N
South Viking Graben
(Vilje sub-basin)
1S
7
GF
BFC
BFS
5 km
2840
Depth (ms TWT)
4648
(B)
N
Fig. 6B
Fig. 6C
GF
3
1S
7
South Viking Graben
(Vilje sub-basin)
BFC
Fig. 6A
BFS
extent of seismic
interpretation
5 km

Fig. 6

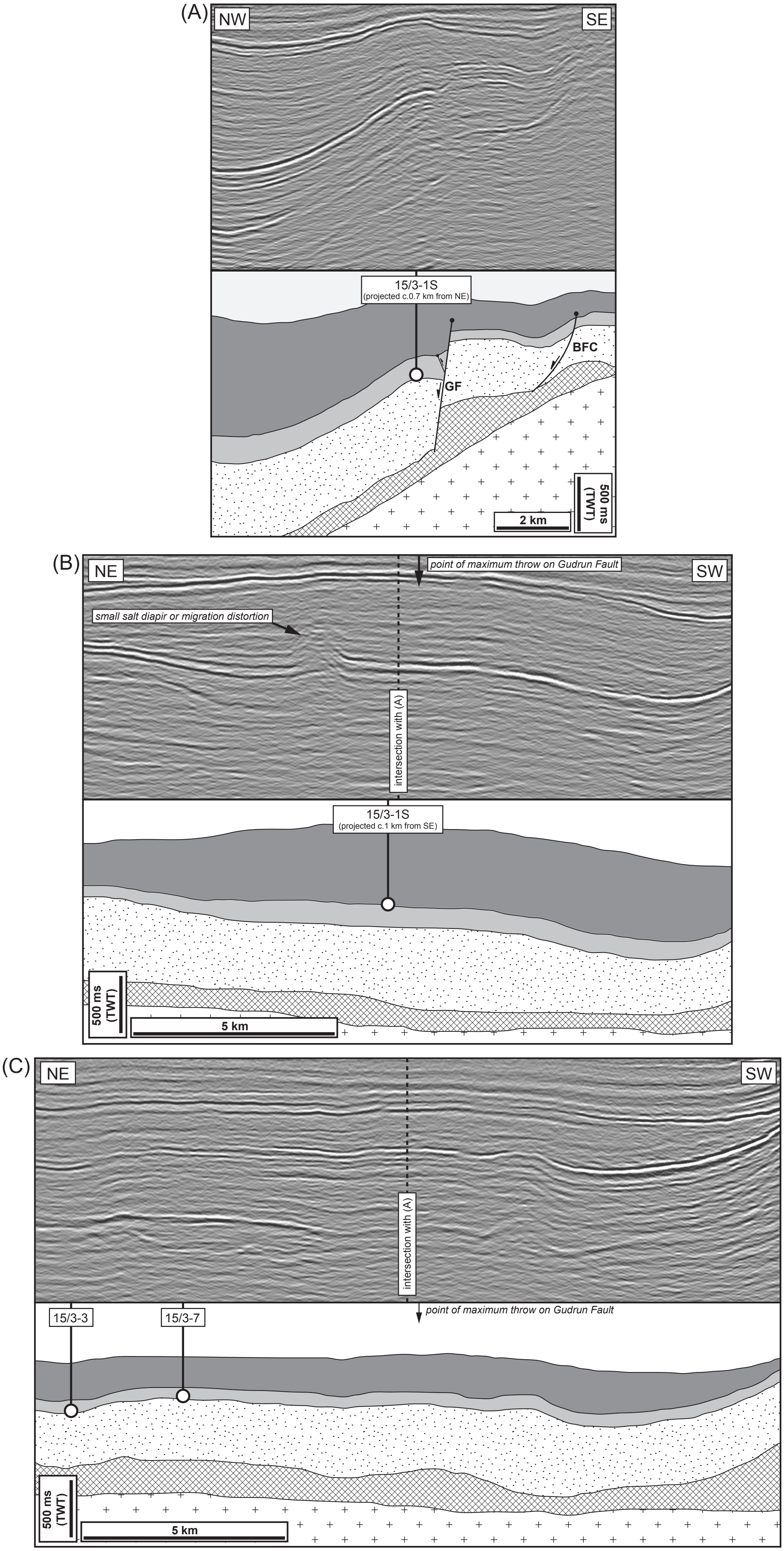

(A)
NW
SE
15/3-1S
(projected c.0.7 km from NE)
GF
BFC
500 ms (TWT)
2 km
(B)
NE
SW
point of maximum throw on Gudrun Fault
small salt diapir or migration distortion
intersection with (A)
15/3-1S
(projected c.1 km from SE)
500 ms (TWT)
5 km
(C)
NE
SW
intersection with (A)
point of maximum throw on Gudrun Fault
15/3-3
15/3-7
500 ms (TWT)
5 km

Fig. 7

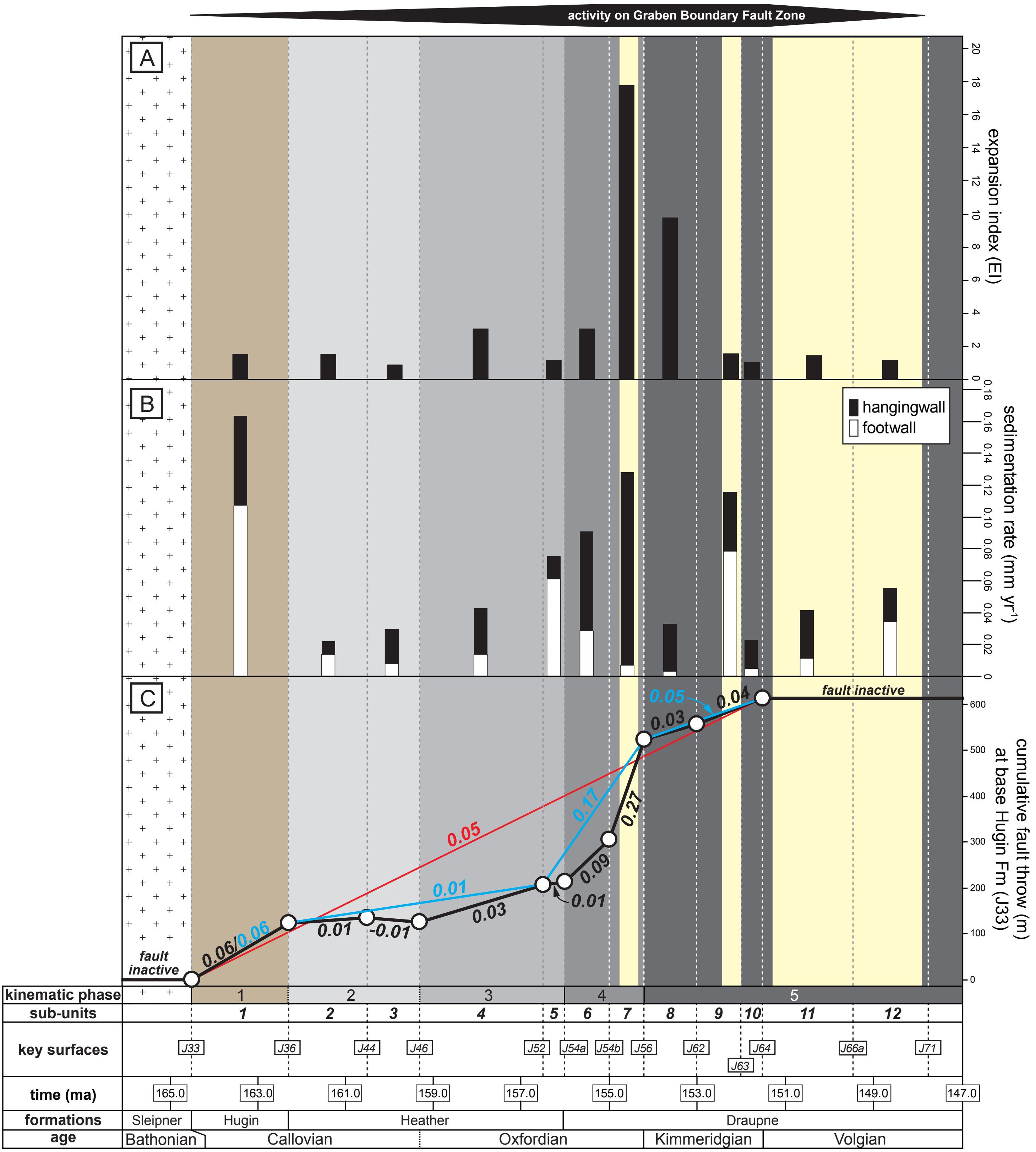

activity on Graben Boundary Fault Zone
A
expansion index (EI)
B
hangingwall
footwall
sedimentation rate (mm yr⁻¹)
C
fault inactive
fault inactive
0.06/0.06
0.01
-0.01
0.01
0.03
0.05
0.01
0.09
0.17
0.27
0.05
0.03
0.04
cumulative fault throw (m) at base Hugin Fm (J33)
kinematic phase
sub-units
key surfaces
time (ma)
formations
age
J33
J36
J44
J46
J52
J54a
J54b
J56
J62
J63
J64
J66a
J71
165.0
163.0
161.0
159.0
157.0
155.0
153.0
151.0
149.0
147.0
Sleipner
Hugin
Heather
Draupne
Bathonian
Callovian
Oxfordian
Kimmeridgian
Volgian

Fig. 8

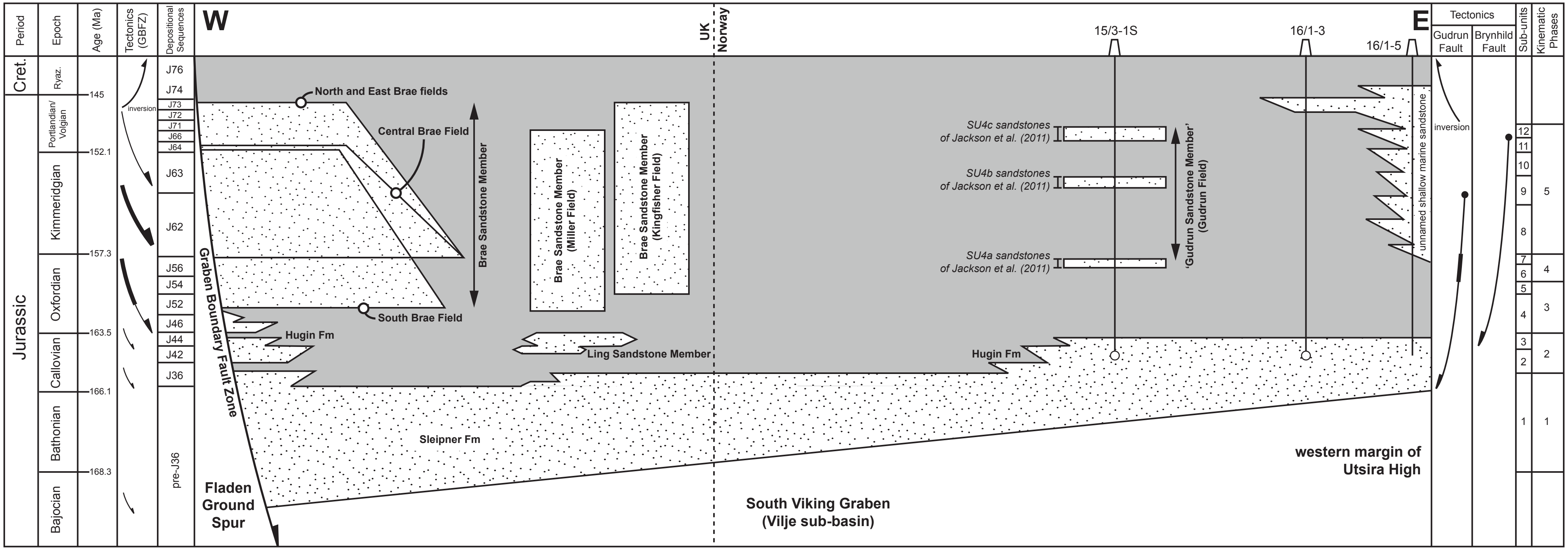

Period
Epoch
Age (Ma)
Tectonics (GBFZ)
Depositional Sequences
W
UK
Norway
E
Tectonics
Gudrun Fault
Brynhild Fault
Sub-units
Kinematic Phases
15/3-1S
16/1-3
16/1-5
Cret.
Jurassic
Ryaz.
Portlandian/ Volgian
Kimmeridgian
Oxfordian
Callovian
Bathonian
Bajocian
145
152.1
157.3
163.5
166.1
168.3
inversion
J76
J74
J73
J72
J71
J66
J64
J63
J62
J56
J54
J52
J46
J44
J42
J36
pre-J36
North and East Brae fields
Central Brae Field
South Brae Field
Brae Sandstone Member
Brae Sandstone Member (Miller Field)
Brae Sandstone Member (Kingfisher Field)
Hugin Fm
Ling Sandstone Member
Graben Boundary Fault Zone
Sleipner Fm
Fladen Ground Spur
South Viking Graben (Vilje sub-basin)
SU4c sandstones of Jackson et al. (2011)
SU4b sandstones of Jackson et al. (2011)
SU4a sandstones of Jackson et al. (2011)
'Gudrun Sandstone Member' (Gudrun Field)
unnamed shallow marine sandstone
western margin of Utsira High
12
11
10
9
8
7
6
5
4
3
2
1